JOURNAL OF MATERIALS SCIENCE 14 (1979) 728–736

The influence of non-uniform incident flux upon surface erosion processes

G. CARTER, M. J. NOBES, K. I. ARSHAK, R. P. WEBB, D. EVANSON, B. D. L. EGHAWARY, J. H. WILLIAMSON
Department of Electrical Engineering, University of Salford, Salford, UK

The surface topographic development by sputter erosion of a solid resulting from spatially non-uniform projectile bombardment is considered theoretically. It is shown that whilst formal prediction of time-dependent surface geometry is possible, analytic solution of the defining equations is generally unachievable, although an approximate treatment may be made for the case of a Gaussian flux distribution profile and an initially plane surface. It is shown that profile perturbations resulting from erosion rate-projectile incidence angle variations can assume importance when erosion crater depths become of similar order to projectile beam width. This behaviour is also revealed by computer simulation of the erosion process and a sand blasting experimental analogue study.

1. Introduction

Energetic projectile beams are being used increasingly for the controlled erosion of solid surfaces in applications such as micromachining of relief patterns on electronic optical and accoustic components, micropolishing (see e.g. [1]) and the removal of reproducible thin layers for composition analysis via ion scattering, secondary ion mass spectrometry, optical photon emission, Auger electron spectroscopy and X.P.S. techniques (see e.g. [2]). In many of these applications the incident projectile flux is either arranged to be spatially uniform or the flux is spatially swept to compensate for local inhomogeneities. Such possibilities are not always applicable, however, whilst in a recent study [3] the projectile flux was deliberately arranged to be spatially inhomogeneous so that the sputter-eroded crater was of variable depth and composition profiling across the crater allowed equivalent depth profiling.

Changes in surface profiles during sputter erosion result, however, not only from projectile flux non-uniformity, but also from the fact that the sputtering rate is generally a function of the angle of incidence of the flux to a surface element (see e.g. [4]). Substantial theoretical and experimental studies of the effects of incidence angle variation of sputtering yield upon the development of surface morphology have been undertaken and reviewed recently [5, 6], but it has been generally assumed that the incident flux is spatially uniform. It is the purpose of the present communication to present a general theoretical study for the case of spatially variable flux, to analyse the development of a crater upon an initially flat surface exposed to a projectile flux with a Gaussian distribution employing computational techniques and to compare the results with an experimental study.

2. Theoretical background

If a local projectile flux Φ per unit area is incident upon a surface element inclined with specific direction cosines to the direction of the flux, then the rate of erosion of the element in a direction normal to the element is given by $\Phi S/N$, where S, the sputtering yield, is a function of the direction cosines and N is the solid atomic density. Although it is possible to study three-dimensional surfaces by vector algebra, it is easier, in a first analysis, to consider a two-dimensional surface generator of the solid in the $x0y$ plane with the projectile flux incident in the y direction and where this flux is

a function of x only. If a random isotropic solid is assumed, then the sputtering yield S will generally be a smooth function of the angle θ between the $0y$ direction (the projectile flux direction) and the normal to a surface element and not exhibit discontinuities due to crystallographic effects. If there are no other processes influencing surface erosion, such as atomic diffusion, evaporation, re-deposition of sputtered atoms or spatial variations in projectile fluence resulting from surface scattering, then the rate of erosion of the surface at a point (x, y) in the normal direction is given by [5]

$$\rho = \frac{\partial n}{\partial t} = -\frac{\Phi(x)}{N} S(\theta) \cos\theta \qquad (1)$$

whilst the rate of erosion in the y direction, at constant x, is given by

$$\left|\frac{\partial y}{\partial t}\right|_x = -\frac{\Phi(x) S(\theta)}{N}. \qquad (2)$$

By considering the relative erosion of neighbouring surface points it is readily shown that the components of the velocity of motion of a surface element which maintains a constant orientation θ are given by

$$\left|\frac{\mathrm{d}x}{\mathrm{d}t}\right|_\theta = -\left|\frac{\partial\theta}{\partial t}\right|_x \Big/ \left|\frac{\partial\theta}{\partial x}\right|_t = \frac{\cos^2\theta}{N} \frac{\mathrm{d}}{\mathrm{d}\theta}\{\Phi(x)S(\theta)\} \qquad (3)$$

and

$$\left|\frac{\mathrm{d}y}{\mathrm{d}t}\right|_\theta = -\left|\frac{\partial\theta}{\partial t}\right|_y \Big/ \left|\frac{\partial\theta}{\partial y}\right|_t = \frac{1}{N}\left\{\sin\theta\cos\theta \frac{\mathrm{d}}{\mathrm{d}\theta}(\Phi(x)S(\theta)) - \Phi(x)S(\theta)\right\} \qquad (4)$$

The resultant velocity of points of constant orientation is then readily derived by vector summation and the direction of motion of such points deduced by division of Equation 3 and 4.

The rate of change of the radius of surface element maintaining constant orientation is given by

$$\left|\frac{\partial R}{\partial t}\right|_\theta = \frac{1}{N}\left\{\frac{\mathrm{d}^2}{\mathrm{d}\theta^2}(\Phi(x)S(\theta))\cdot\cos\theta - 2\frac{\mathrm{d}}{\mathrm{d}\theta}(\Phi(x)S(\theta))\cdot\sin\theta\right\}. \qquad (5)$$

It may be noted that Equations 1 to 5 are generalizations for variable $\Phi(x)$ of corresponding equations for constant Φ [5] and are readily derivable by replacing $\Phi \cdot S(\theta)$ in earlier studies [5] by $\Phi(x)S(\theta)$. Although derivation of these equations is straightforward, their solution to provide the time dependent (x, y, θ) contour is difficult except for trivial cases such as S independent of θ. Consequently, either numerical computational methods or graphical methods must generally be employed. Thus for the case of uniform flux, Equation 1 has to be solved numerically [7–9] in an iterative manner to deduce the change in a sinusoid wave form surface as a function of time. This method will be employed subsequently to study the erosion of an initially plane surface exposed to a non-uniform Gaussian distributed projectile flux.

One of the geometric techniques for following the progress of points of constant orientation [5, 10] is to plot, for uniform projectile fluence, an "erosion slowness" curve which is the behaviour of $1/(\Phi \cdot S\cos\theta)$ as a function of θ. The trajectory of any point of orientation θ on the eroding real surface is then parallel to the normal to the erosion slowness curve and the erosion velocity is equal to the reciprocal of the length of the normal from the origin of the erosion slowness curve. In the case of non-uniform flux, $\Phi(x)$, a family of erosion slowness curves appropriate to all values of $\Phi(x)$ can be similarly constructed and, for an initial surface profile, an effective erosion slowness curve appropriate to each surface point value of $\Phi(x)$, x and θ constructed through the family of curves. The motion of each surface point over a small time increment may then be deduced from the normals to this effective erosion curve and the new surface profile determined. This new initial condition may then be employed to deduce a new effective erosion slowness curve appropriate to the values of $\Phi(x)$, x and θ at time δt, and this in turn employed for a second time step. Further iteration then follows the same process, with care exercised, as is the case for uniform flux conditions and in numerical computation methods, when zero radius edges form during the erosion sequence.

Before considering the specific case of an initially plane surface exposed to a Gaussian flux distribution in detail, however, we may note the relative importance of flux non-uniformity and the angular variation of sputtering yield in determining

the time-dependent surface profile development. The local profile perturbation due to differential erosion processes may be evaluated by differentiating Equation 2 with respect to x, i.e.

$$\frac{\partial}{\partial x}\left(\frac{\partial y}{\partial t}\right) \equiv \frac{\partial}{\partial t}\left(\frac{\partial y}{\partial x}\right) = -\frac{1}{N}\frac{\partial}{\partial x}\{\Phi, S\}$$

$$= -\frac{1}{N}\left\{\frac{\partial \Phi}{\partial x}\cdot S + \Phi\frac{\partial S}{\partial \theta}\cdot\frac{d\theta}{dx}\right\}. \quad (6)$$

The first term on the right-hand side of Equation 6 describes the differential erosion process due to flux inhomogeneity, whilst the second term describes the process resulting from incidence angle sputtering yield variations. It is thus possible, in general terms, to deduce that, for any arbitrary initial profile, flux inhomogeneity is the dominant perturbational influence for surface points where the values of x, θ, $d\Phi(x)/dx$ and $dS(\theta)/d\theta$ are such that

$$S(\theta)\frac{d\Phi(x)}{dx} \gg \Phi(x)\frac{dS(\theta)}{d\theta}\cdot\frac{d\theta}{dx}, \quad (7)$$

whereas incidence angle sputtering yield variation is dominant when the inequality of Equation 7 is reserved. As erosion continues, however, then, at any given x (or θ) value the relative magnitudes of the two components will change continuously. Consequently, it is impossible, except under quite specific conditions, to define the major perturbational influence. One such case is that of an initially plane surface normal to the projectile flux direction which we shall discuss fully shortly. In this case, θ is initially, and for small times, zero or close to zero, $d\theta/dx$ is small and $S(\theta)$ is approximately constant at $S(\theta)$. Thus the flux inhomogeneity term is dominant and the eroded depth at a given spatial point x is approximately directly proportional to the flux at that point.

With increasing time, however, as θ and $d\theta/dx$ increase, the sputtering yield–incidence angle variation term assumes importance. The *approximate* stage at which this occurs may be deduced as follows. In a small angle approximation $dy/dx = \tan\theta \approx \theta$ and Equation 6 becomes

$$\frac{\partial \theta}{\partial t} = -\frac{1}{N}\left\{\frac{d\Phi}{dx}\cdot S + \Phi\frac{dS}{d\theta}\cdot\frac{d\theta}{dx}\right\}. \quad (8)$$

If, initially, the flux inhomogeneity term dominates, then Equation 8 may be integrated to give

$$\theta \approx -\frac{1}{N}\frac{d\Phi}{dx}\cdot St, \quad (9)$$

and hence

$$\frac{\partial \theta}{\partial x} \approx -\frac{1}{N}\frac{d^2\Phi}{dx^2}\cdot St. \quad (10)$$

Thus, the time, τ, at which the two terms of Equation 6 become equal is given by

$$S\frac{d\Phi}{dx} \approx -\frac{\Phi}{N}\frac{dS}{d\theta}\frac{d^2\Phi}{dx^2}S\tau$$

or

$$\tau \simeq -\frac{d\Phi/dx}{\Phi(dS/d\theta)\cdot d^2\Phi/dx^2} = \frac{1}{N}. \quad (11)$$

τ can only be evaluated if the angular variation of S is known (e.g. for small angles $S(\theta)\approx S(o)\sec\theta$) and a specific form for $\Phi(x)$ is assumed so that the $\theta - x$ relationship may be deduced from Equation 9 and hence $dS/d\theta$ can be determined as a function of x and τ.

In a small angle approximation and with $S \approx S(o)\sec\theta \approx S(o)(1+\theta^2/2)$, then $dS/d\theta \approx S(o)\cdot\theta$, and thus, from Equation 9

$$\frac{dS}{d\theta} \approx -\frac{1}{N}\frac{d\Phi}{dx}S(o)^2 t. \quad (12)$$

Consequently,

$$\tau \approx \frac{N^2 d\Phi/dx}{S(o)^2\Phi\cdot d\Phi/dx\cdot d^2\Phi/dx^2\cdot\tau}$$

or

$$\tau \approx \frac{N}{S(o)}\left\{\left|\frac{1}{\Phi(d^2\Phi/dx^2)}\right|\right\}^{1/2}. \quad (13)$$

If a Gaussian distributed flux profile, which should be a reasonable approximation to a typical experimental projectile beam, is assumed, with the form

$$\Phi(x) = \Phi(o)\exp -\frac{x^2}{2\sigma^2}, \quad (14)$$

then Equation 13 reveals that the time constant τ is a minimum at $x = 0$.

The eroded depth, at time τ, is given by $y_\tau = \tau\cdot\Phi S(o)/N$, which, from Equation 13 is

$$y_\tau = \left\{\left|\frac{\Phi}{d^2\Phi/dx^2}\right|\right\}^{1/2}. \quad (15)$$

At the centre ($x = 0$) of a Gaussian distributed flux, Equation 15 indicates that $y_\tau \approx \sigma$, the

standard deviation of the flux profile. Thus, in order for incidence angle sputtering yield variation processes to assume importance, the central crater eroded depth must be of the order of the flux profile width. Generally speaking, for depth analysis studies the sputtering projectile beam width will be of the order of 1 mm, whilst eroded depths will be of the order of hundreds of thousands of Ångstrom units. In such studies, therefore, the erosion crater profile will be almost completely dictated by the beam profile inhomogeneity.

In micromachining applications, however, where both beam dimensions and crater depths are of the order of microns, the incidence angle sputter yield variation process will assume considerable importance in determining crater profiles, and indeed this may be observed to be true from studies [11] of crater profiles which are of trapezium rather than rectangular section, with side face angles which correspond to those dictated by incidence angle–sputter yield processes.

However, the approximations leading to Equation 15 ignore the higher order terms of θ in the $S(\theta)$ and $dS(\theta)/d\theta$ expansions and may, therefore, be taken only as indicative rather than prescriptive. In order to be more precise in defining the role of incidence angle sputtering yield variations it is necessary to employ computational methods to which we shortly turn attention.

We may note one important property of non-uniform flux irradiation, however, which is that a stable equilibrium time independent form is generally unlikely to form, in contrast [5] to the uniform flux irradiation where stable time independent geometry is possible for $\theta = 0$ (normal to the projectile flux) and $\theta = \pm\theta_p$ (the angles at which the S–θ function exhibits maxima).

This inability to approach equilibrium may be perceived from Equation 6 which reveals that a spatial independence of $\partial y/\partial t$ requires that the product $\Phi(x) \cdot S(\theta)$ must be constant everywhere on the irradiated surface. Since, for given projectile–substrate parameters the S–θ function is fixed and may be represented, for example, by a polynomial function of θ, then for each x co-ordinate, corresponding to a given local flux $\Phi(x)$, a value of θ may potentially be derived from solution of the equation

$$S(\theta) = \frac{\text{constant}}{\Phi(x)}. \qquad (16)$$

Since the $S(\theta)$ function is a fixed form, however, it is generally probable that a solution for θ could not be achieved over the full range of $\Phi(x)$ (this is specifically true if, anywhere $\Phi(x) = 0$ since $S(\theta)$ can never be infinite and includes the case of the Gaussian flux distribution). A specific form of $\Phi(x)$ for which equilibrium could be achieved everywhere upon the surface would be when this distribution was of a form which was the inverse of the shape of the S–θ function. Equilibrium may also be possible for a *finite* surface, within which $\Phi(x)$ is nowhere zero and then the stable form would mirror the surface of Equation 16 over a restricted range of θ values.

3. Computational studies

In order to explore the validity of the preceding, approximate analysis, a computer simulation model was set up. In this model the time step variation of the surface contour was followed assuming an initial condition of a plane surface exposed to a Gaussian flux profile and with an S–θ curve shown in Fig. 1. Both the S–θ function and the Gaussian profile were chosen to match *closely* to experimentally derived functions which are described in the next section and could be cast in analytic function form (which the experimental data could not) for computational convenience. Thus the forms chosen for $S(\theta)$ and $\Phi(x)$ were

$$\frac{S(\theta)}{S(o)} = 33.5\cos\theta - 90.9\cos^2\theta + 93\cos^3\theta - 34.6\cos^4\theta \qquad (17)$$

$$\frac{\Phi(x)}{\Phi(o)} = \exp(-x^2/2\sigma^2). \qquad (18)$$

The time step between calculations was set to the amount of time taken to remove a 200th part of a standard deviation at the maximum and all distances were put in units of σ, thereby making the data independent of the actual value of σ. For computational convenience, the Gaussian profile was cut off to zero at $x = \pm 3\sigma$, and so there are *small* errors in the derived form of the resulting crater profile for $x < \pm 3\sigma$ and for $x > \pm 3\sigma$. The interval $-3\sigma < x < +3\sigma$ was then divided into 80 segments and the change in the (x, y) co-ordinates at each of these initially selected x co-ordinates was computed in an erosion time step. As will be seen later, the erosion flux distribution was itself not measured directly, but the depth eroded in the $0y$ direction per unit time (i.e

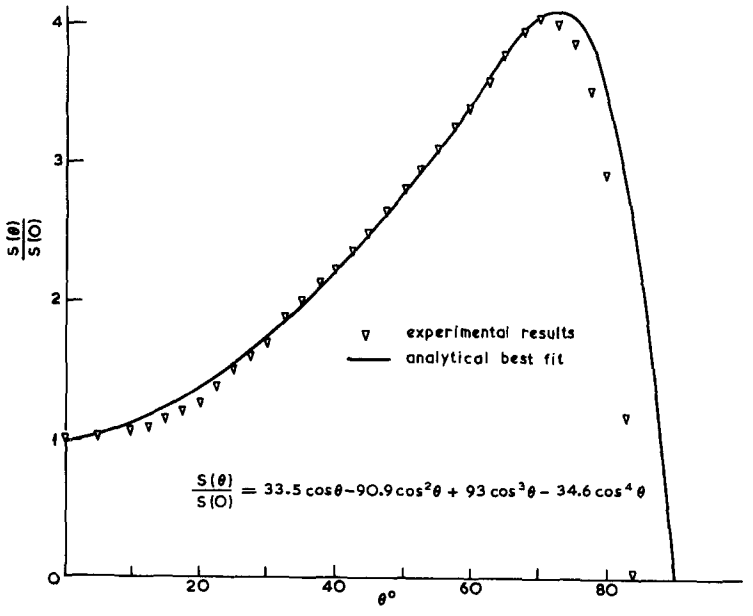

Figure 1 Normalized erosion rate as a function of incidence angle.

1 min) was evaluated for short times where $S(\theta)$ variations are unimportant on an initially plane surface. Thus, the short time experimental data effectively yields the function

$$-\frac{\delta y(x)}{\delta t} = \frac{\Phi(x) \cdot S(\mathrm{o})}{N}. \qquad (19)$$

In addition, the experimental data did not yield directly the number of surface atoms ejected per incident projectile as a function of incidence angle θ (the definition of $S(\mathrm{o})$), but measured the weight loss of a sample for constant projectile fluence at various incidence angles. This weight loss curve was normalized to the value at $\theta = 0$, so that, as also shown in Fig. 1, the form of $S(\theta)/S(\mathrm{o})$ as a function of θ was derived. Thus, as erosion of the solid proceeded, the erosion rate at any surface point was determined from the product of the small time erosion rate $(-\delta y/\delta t)$ and the ratio $S(\theta)/S(\mathrm{o})$ appropriate to the angle θ at the point on the surface under consideration.

The detailed programme proceeded as follows. At time $t = 0$, the changes δx_n and δy_n in the $(x_n, y_n = 0)$ values between $\pm 3\sigma$ were computed for a time step equilavent to a maximum erosion of $\sigma/200$ in the y direction. The value of δy_n was derived from $-\delta y_n \cdot 1/\delta t$ and the value of δx_n from $-\delta y_n \cdot \tan\theta/\delta t$, which, as readily shown [5] from Equation 1 describes point motion in the x direction when actual motion is normal to the surface. These values of δx_n, δy_n were then used to reconstruct the new surface profile at $t = 1$. The new values of y_n and x_n were then used to construct the new surfaces. After profile construction the values of θ_n appropriate to the new x_n were evaluated from

$$\tan\theta_n = \frac{y_{n+1} - y_{n-1}}{x_{n+1} - x_{n-1}}. \qquad (20)$$

The erosion process was then repeated for a further time step, for each value of x_n, by multiplying the zero angle ($\theta = 0$) erosion rate ($= \delta y_n/\delta t$) by the value $S(\theta_n)/S(\mathrm{o})$ at that point. As the surface regressed, new points were added to supplement those moving away from the peak. By following this process sequentially, the profile of the erosion crater could be determined after a given number of time steps and Fig. 2 illustrates the results so obtained after time steps of 1, 100, 200 and 500. For the shorter times the resulting curves, which are normalized to the maximum eroded depth at $x = 0$, were found to be almost indistinguishable and reflect the image of the initial flux profile. With increasing time, however, the form of the profile changes significantly and the long time curves in Fig. 2 (i.e. maximum eroded depths of $\frac{1}{2}\sigma$, σ, 2.5σ) have been chosen to represent the cases where the maximum erosion depth becomes of the order of and greater than the standard deviation, σ, of the flux profile. From these curves, therefore, it is apparent, as approximately predicted earlier, that departures from a flux profile-dictated crater profile geometry do occur when the eroded depth is of the order of σ.

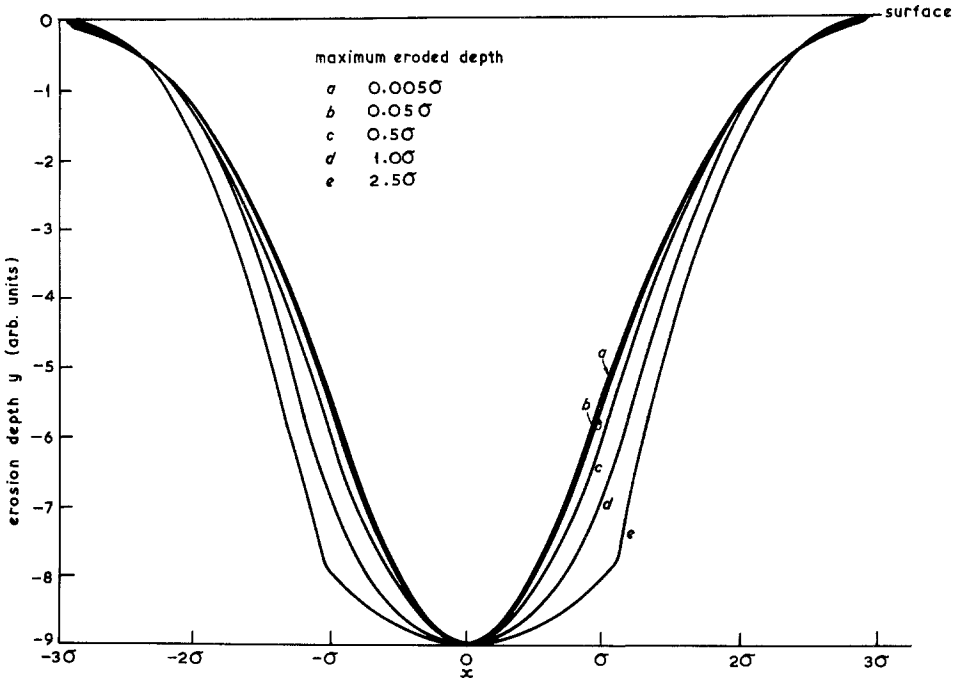

Figure 2 Computed erosion crater profiles (normalized at maximum depth of erosion) for a Gaussian flux profile and the best fit erosion rate–incidence angle function of Fig. 1.

At still larger times than those depicted in Fig. 2, it was observed that using the programme outlined above, oscillations in the crater profile near the maximum eroded depth were predicted by the simulation. It was quickly discovered that this behaviour resulted from crossings of the erosion trajectories of neighbouring x_n points on the profile resulting in the unphysical but mathematically possible cusps on the surface. This problem has been recognized in similar (but homogeneous flux) simulations by other authors [8, 9] and arises from the formation of edges or discontinuities (which are the precursors of cusps) via intersecting erosion trajectories. As indicated in [5] and [10], the motion of such discontinuities must be treated cautiously and separately from points on a continuous curve by appeal to the erosion slowness curve. In order to recognize the initial formation of such discontinuities, the programme was revised so that if, using the 1 unit time step schedule, a profile indicating a cusp formation occurred at a given stage the programme reverted to an earlier time and then continued with much shorter time steps until the discontinuity appeared. The motion of this and any subsequent discontinuities was then followed using the required information from the erosion slowness curve moderated by the local flux $\Phi(x_n)$ at and near the discontinuity. By following this procedure, smoother profiles were obtained as erosion continued, but as indicated earlier would be the case, no final equilibrium form was deduced, the profile deepening and broadening (within the cut-off at $\pm 3\sigma$ constraint) continuously. The results of these longer time simulations are shown in Fig. 3, for maximum eroded depths up to 3.5σ, and it is becoming apparent from these non-normalized curves that the general character of the erosion profile changes towards a flattish bottom crater with steeply rising sides with the elevation angle of this inverted and truncated approximately conical shape tending to about 68°. This is similar, but not identical, to the value of θ in Fig. 1, at which the erosion rate is a maximum. As we will see later, the general form of the changing crater profile determined computationally is quite similar to that observed experimentally.

4. Experimental studies

Although the major interest of our work is to study and understand the effects of non-uniform ion beams upon surface sputtering erosion, it was clearly recognized that in *most* applications the effects of S/θ variations would be minimal since

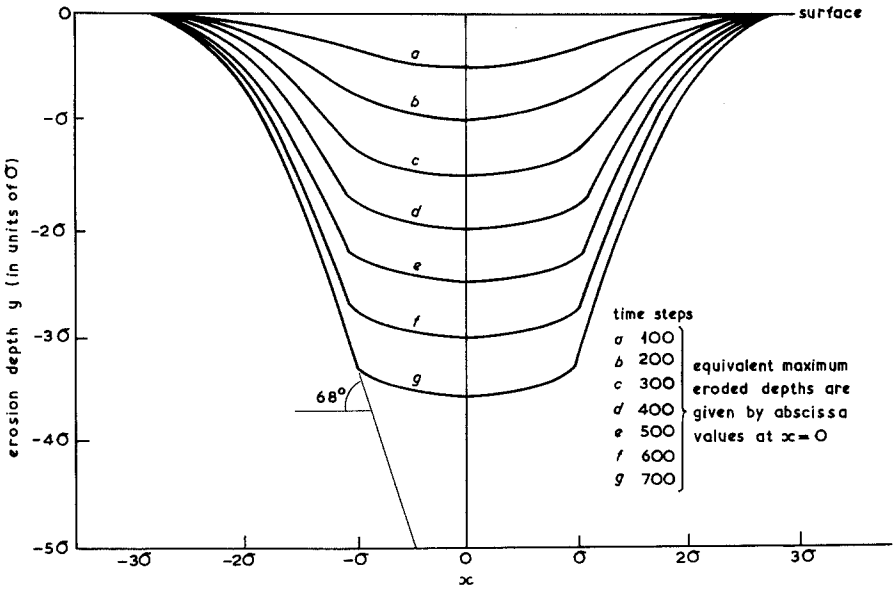

Figure 3 Computed erosion crater profiles (non-normalized), with same conditions as in Fig. 2 but for increasing erosion stages.

crater depths would be very much less than the beam width, excepting the cases of micron-sized beams which were not readily at our disposal. Thus, if the effects predicted earlier were to be perceived with a 1 mm diameter beam (available from our accelerator), then even with the highest beam intensity ($\simeq 10\,\mathrm{m\,cm^{-2}}$) and a favourable sputtering ratio ($S(\mathrm{o}) \simeq 10$) would have required several hours' bombardment to develop a crater depth of the order of 1 mm. It would also have been necessary to measure carefully the $S(\theta)$ function for the chosen substrate–radiation conditions. In order to model the ion erosion process on a more acceptable time scale, therefore, a more aggressive erosion process was adopted, that of "sandblasting".

Although the processes of erosion of material from solids by energetic ions and fluid-entrained small macroscopic particles are almost certainly different, there is an important analogue of product, additional to the total ablation itself. Thus, it is well established [12, 13] that the erosion rate of a ductile solid (as measured by weight loss or depth eroded) is a *very similar* function of macroparticle impingement angle to the surface normal, as is the S/θ function of ion bombardment sputtering of isotropic solids. Moreover, high flux commerically available sandblasters generally give rise to surface removal rates of millimetres per hour and the flux distribution profile emerging from the sand blaster nozzle is often highly inhomogeneous. This process was, therefore, chosen to analogue model the ion sputtering effect.

Experimentally, a flux of 30 μm mean diameter alumina particles was directed onto polycrystalline Cu surfaces held at a distance of about 2 cm from the nozzle of an S.S. White Airbrasive unit. The samples were of substantially larger area than the particle beam dimensions. Initially the erosion rate/incidence angle function was determined following erosion for fixed, long times (~ 10 min) by weight loss measurements using a simple laboratory balance. It was also checked that, for each angle of incidence, the weight loss was a linear function of erosion time. From these measurements the percentage weight loss was derived as a function of incidence angle and normalized to the value at perpendicular incidence to give the "experimental" curve of Fig. 1. The form of this erosion rate curve is similar to both ion sputtering data [1] and to earlier studies of sandblast erosion of ductile solids [12, 13]. Next, using identical erosion conditions, and normal incidence on the Cu surface, erosion was continued, at a number of different points on the surface for different, increasing times between 1 and 100 min. The profile of the crater was then deduced, for the shorter times, by traversing across the crater with a Rank-Taylor Hobson "Talysurf"

instrument (which has a depth resolution of $\sim 2 \times 10^{-8}$ m) and for longer times where eroded depths were of millimetre dimensions by making a dental resin of the crater and using a magnified optical shadowcasting technique. The two techniques were shown to give equivalent crater profiles at intermediate times where both were applicable.

The results of these measurements are shown in Fig. 4 normalized at the crater maximum depths which correspond to values of 0.075σ, 0.275σ, 2.5σ and 4σ. For the shorter erosion times, the normalized erosion centres are essentially identical and thus reflect the incident projectile flux profile. As indicated in Fig. 4, this profile is not quite Gaussian when compared with the closest matched Gaussian approximation, used in the computer simulations, and also shown on Fig. 4.

Measurement of the maximum erosion depth (at $x = 0$) as a function of erosion time showed these to be closely linearly related, thus indicating that the deepest part of the crater maintains an angle of $\theta \approx 0^\circ$ for all erosion times. This result also suggests that secondary effects, such as differential flux enhancement, resulting from eroded particle reflection and reimpingement and eroded material deposition were largely absent and indicates the validity of neglecting these processes in the numerical simulation. In ion irradiation studies, such secondary effects have been noted [5] and would require a more detailed analysis than is presented here. For larger erosion times the crater profile begins to exhibit a marked departure from the short time shape and, as can be seen in Fig. 4, this departure becomes evident when the maximum eroded depth is of order σ. These experimental studies support the theoretical and computational conclusions reached earlier. Since in the computational simulation neither the $\Phi(x)$ nor $S(\theta)$ functions precisely match the experimental data we will not attempt to compare quantitatively the experimental measurements and the simulation prediction. It is quite clear qualitatively, however, that the general shape change, towards a flattish bottom, quasi conical crater, as measured experimentally, is very similar to that predicted computationally and it may be noted that, again, the elevation angle of the quasi conical portion of the profile is about 70°. As shown in Fig. 3, the numerical calculations indicate that the area of flattish part of the crater base (which is maintained in shape similar to the short erosion time profile) gradually decreases with increasing erosion time, and, whilst this is not apparent in the normalized data of Fig. 4 (cf. Fig. 2), the actual experimental profiles (non-normalized) also reveal this effect. This is understandable since major shape changes would be expected to occur first, due to S–θ variation effects, where large slope angles first occur (i.e. near $x = \pm\sigma$, where $d\Phi/dx$ is a maximum) rather than near the crater base where $\theta \approx 0^\circ$ and $d\Phi/dx = 0$. As erosion proceeds, however, the S–θ variation will increasingly influence the region near $x = 0$ as larger slope angles develop inwards from $x = \pm\sigma$ towards $x = 0$, thus leading to a contraction of the flattish area and an expansion of the steeply sloping area. Although, in the stages of development studied, there is a clear tendency for major portions of the crater profile to develop angles near to $\theta = \theta_p$, then the maximum erosion rate occurs, and this is entirely expected upon erosion rate theoretical

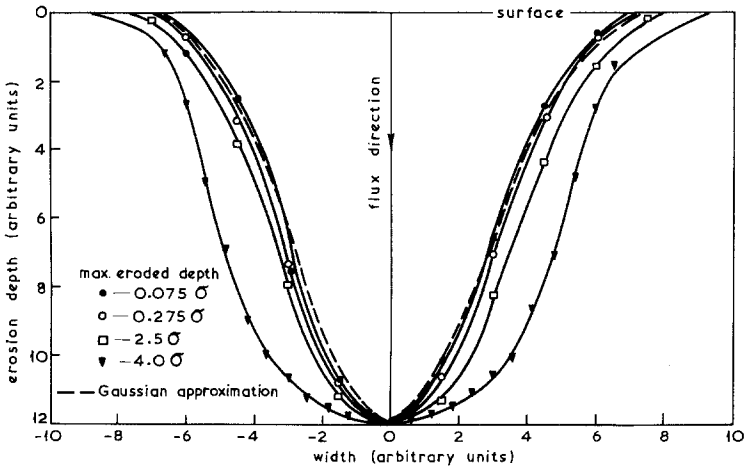

Figure 4 Sandblast erosion crater profiles (normalized at maximum depth of erosion).

grounds [5], it is suggested that this is only a transient process since, as argued earlier, no true equilibrium can be achieved for a non-uniform flux profile. Nevertheless, the results do show clearly the increasing dominance of the $S-\theta$ variation (as reflected by this tendency to form profiles with $\theta \approx \theta_p$) over the flux variation and this factor must, therefore, be carefully considered in deep profile etching.

Although we have considered here only a special case of a Gaussian flux distribution and an initially flat surface, the arguments and techniques presented are equally applicable to other situations and it is suggested that the type of numerical modelling outlined here should be applied to such situations to predict the form of topography development rather than assuming that surface profiles will mirror the projectile flux profile.

5. Conclusions

In this study we have shown that theoretical, computer simulation and sandblasting analogue experimental simulation of the development of profiles on surfaces sputtered (eroded) by spatially non-uniform projectile beams are influenced by the variation of erosion rate with projectile incidence direction. These effects are unimportant when only minor erosion of a plane surface occurs since the incidence angle remains roughly constant. Where either the eroded depth is comparable to the spatial dimensions of the projectile flux, so that large incidence angles can develop, or where such large angles initially exist upon a surface, however, the erosion rate incidence angle variations can lead to substantial perturbations in the surface profile from that anticipated solely on the basis of projectile flux non-uniformity. Such effects are, therefore, unlikely to be important for techniques which employ sputter etch depth profiling to deduce near surface ($\leqslant 1000$ Å) concentrations of impurities in solids using broad ion beams ($\gg 1000$ Å) but can assume importance in micro-machining applications, where etch depths are similar to beam profile dimensions if the flux in such beams are non-uniform. It may also be concluded that similar effects would assume importance in more macroscopic surface ablation processes (sandblasting was illustrated here).

References

1. E. G. SPENCER and P. H. SCHMIDT, *J. Vac. Sci. Technol.* 8 (1971) 522.
2. P. S. HO, J. E. LEWIS, H. S. WILDMAN and J. K. HOWARD, *Surface Science* 57 (1976) 393.
3. H. W. WERNER, Conference on Ion Sputtering and Surface Analysis, 1977. Institute of Physics (Thin Films Group) London (unpublished).
4. H. OECHSNER, *Appl. Phys.* 8 (1975) 185.
5. G. CARTER, J. S. COLLIGON and M. J. NOBES, *Rad. Effects* **31** (1977) 65.
6. G. CARTER, M. J. NOBES, J. L. WHITTON, L. TANOVIC and J. S. WILLIAMS, Proceedings of the VII International Conference on Atomic Collisions in Solids, Moscow, 1977 (to be published).
7. C. CATANA, J. S. COLLIGON and G. CARTER, *J. Mater. Sci.* 7 (1972) 467.
8. T. ISHITANI, M. KATO and R. SHIMIZU, *ibid.* 9 (1974) 505.
9. J. P. DUCOMMUN, M. CANTAGREL and M. MARCHAL, *ibid.* 9 (1974) 725.
10. D. J. BARBER, F. C. FRANK, M. MOSS, J. W. STREEDS and I. S. T. TSONG, *ibid.* 8 (1973) 103.
11. H. DIMIGEN and H. LÜTHJE, *Phillips Tech. Rev.* 35 (1975) 199.
12. I. FINNIE and Y. H. KABIL, *Wear* 8 (1965) 60.
13. J. G. A. BITTER, *ibid.* 6 (1963) 169.

Received 30 June and accepted 6 September 1978.